Quasi-Lagrangian Kinetic Energy Budgets of Composite Cyclone-Anticyclone Couplets

TAI-JEN GEORGE CHEN[1] AND LANCE F. BOSART

Department of Atmospheric Science, State University of New York at Albany, Albany, N. Y. 12222

(Manuscript received 23 April 1976, in revised form 19 November 1976)

ABSTRACT

A composite quasi-Lagrangian kinetic energy budget is constructed from four synoptically similar cases of polar air penetration into the Caribbean from off the North American continent. Computations were carried out for both the upstream anticyclone and downstream cyclone accompanying the polar outbreak.

Use of the residual technique suggests an average upscale energy exchange of 45.0 W m^{-2} over the anticyclone volume with a corresponding downscale energy transfer of 59.0 W m^{-2} over the cyclone volume for the 24 h period centered on the time of furthest southward cold air thrust as defined by the 1000–500 mb thickness patterns. The results also indicate that the vertical flux of kinetic energy ranges from 50 to 100% of the horizontal flux of kinetic energy and is of opposite sign below 400 mb in the cyclone volume. Furthermore, during incipient surface cyclogenesis the horizontal boundary flux of 17.7 W m^{-2} is a significant fraction of the local kinetic energy generation of 24.5 W m^{-2} whereas in the following 12 h time period these numbers become 32.2 and 64.6 W m^{-2}, respectively. The corresponding figures for the anticyclone region include a horizontal export of kinetic energy of 37.2 and 55.0 W m^{-2} and local kinetic energy destruction of 9.5 and 6.0 W m^{-2}, respectively, for the same 12 h time periods.

1. Introduction

The purpose of this paper is to present a limited-area quasi-Lagrangian kinetic energy budget of a composite of four cyclone-anticyclone couplets during winter over the North American continent. Energetic studies of atmospheric motion systems have become one of the major concerns in understanding the dynamical and physical processes of large-scale weather systems since the early work of Margules (1910) on the energy production of storms. Numerous theoretical and observational studies concerning the large-scale atmospheric energy cycle have been made over the last two decades. Some of these results are summarized and discussed in the papers by Oort (1964), Lorenz (1967), Dutton and Johnson (1967), Johnson (1970), Pearce (1974), Kung and Baker (1975) and Johnson and Downey (1975a, b, 1976).

The present paper focuses on cyclone-anticyclone couplets in the belief that a proper investigation of cyclonic development must also consider the interaction of flanking ridges. The limited area energetics equations formulated by Smith (1969) for an Eulerian system and modified by Vincent and Chang (1973) to a quasi-Lagrangian coordinate system are adopted in the present investigation.

2. Case selection

The data used to generate synoptic cases for the overall composite consisted of surface and upper air charts as well as 1000–500 mb thickness maps as routinely transmitted over the National Weather Service facsimile circuit for the winter season October through March, 1968–72. The 5-year sample period was determined by in-house chart availability. Case selection was restricted to North and Central America and adjacent oceanic regions. These areas have reasonably good coverage and quality of surface and radiosonde observations. Eligible cases were restricted to those involving penetration of cold air from the North American continent deep into low latitudes to the rear of a major cyclone along the east coast of the United States. The cyclone-anticyclone couplets were well-developed in these areas.

An arbitrary and subjective criterion was used in the case selection in that the 1000–500 mb thickness pattern had to exhibit a well-defined baroclinic zone across the Gulf of Mexico and western Caribbean with penetration of the 5640 m thickness line to south of 20°N between 85 and 95°W. These are favorable longitudes for the

[1] Present affiliation: Department of Atmospheric Sciences, National Taiwan University, Taipei, Republic of China.

penetration of cold air into the tropics from the North American continent. Additionally, a surface cold front passage across 15°N was required in the Caribbean in response to a strong anticyclonic push from the north. Sixteen cases were found to satisfy these conditions such that a strong cyclone-anticyclone couplet was observed.

3. Compositing technique

Four cases were finally chosen for compositing on the basis of subjectively determined similarities in the surface and tropospheric flow patterns. Each case consists of eight time periods (times 1–8) at 12 h intervals as follows:

(a) 1200 GMT 10 November 1968 to 0000 GMT 14 November 1968
(b) 1200 GMT 7 February 1971 to 0000 GMT 11 February 1971
(c) 0000 GMT 12 February 1971 to 1200 GMT 15 February 1971
(d) 0000 GMT 19 March 1971 to 1200 GMT 22 March 1971.

For each case the time periods have been relabeled in chronological order as time periods 1–8. The quasi-Lagrangian kinetic energy budget presented in this paper is restricted to time periods 3–5, where time period 4 represents the time of the southernmost penetration of cold air in terms of the observed 1000–500 mb thickness field.

The data used to construct the composite maps consisted of mandatory (every 50 mb) and significant level radiosonde data for 94 stations for each time period for each case covering the area bounded by 40°W, 120°W, 5°N and 50°N. The data were obtained from the Northern Hemisphere Data Tabulations (NHDT) supplemented by surface synoptic and marine observations obtained from the National Climatic Center. Reports from a few upper air observations not routinely available from the NHDT as well as for those stations reporting only mandatory levels were obtained in their entirety from the National Climatic Center. Data were available for only three of the four cases at a total of 15 stations due to errors at the original source or the establishment or closing down of a station during the time period of this study. A linear interpolation procedure was used in both space and time to account for missing observations.

The compositing procedure consisted of a straight average of reported temperatures and relative humidities at the mandatory levels (every 50 mb) along with a vector average for the wind observations plus derivation of an average sea level pressure. Significant level temperatures and relative humidities were incorporated into the compositing procedure as illustrated by the following example: If a significant level was reported (e.g., 875 mb) for time 2 for one particular case, then 875 mb temperature and relative humidity data were derived for the other three cases at the same time period by a pressure-weighted interpolation scheme using the 900 and 850 mb data observed for those cases. The 875 mb data (observed and derived) were then composited exactly like the mandatory level data. This procedure was used for all reported significant level information. Finally, a procedure originally outlined by Duquet (1964) was used to derive the geopotential every 50 mb at each radiosonde station using the known station surface elevation, average surface pressure, and known vertical profiles of temperature and relative humidity.

The authors are well aware that the decision to use composite maps for a data base might be strongly criticized on the grounds that legitimate meteorological gradients tend to be overly smoothed and genuine smaller scale features of the flow patterns partially or totally eliminated. The decision to use the composite approach was predicated by the desire to retain true synoptic-scale features as well as to, hopefully, provide more representative kinetic energy budget calculations. In addition, it is hoped that in the composite case most of the spurious random errors due to observation or processing will be eliminated. The nature of the compositing is such that diurnal variations are also suppressed. Finally, the high degree of similarity between the four cases can be seen by comparing the individual maps for time periods 3–5.

4. Computational method

A quasi-Lagrangian isobaric coordinate system is employed in this paper such that

$$\frac{\delta}{\delta t_p}=\frac{d}{dt}-(\bar{\mathbf{V}}_h-\bar{\mathbf{C}})\nabla_p-(\omega-\omega_B)\frac{\partial}{\partial p}, \tag{1}$$

where $\delta/\delta t_p$ is the local rate of change following the motion of the system, $\bar{\mathbf{V}}_h$ the horizontal wind velocity, $\bar{\mathbf{C}}$ the horizontal system velocity and ω_B the "vertical motion" of the quasi-Lagrangian isobaric coordinate system.

The total kinetic energy of a limited volume per unit area (KE) can be written as

$$\mathrm{KE}=\frac{1}{gA}\int_A\int_{p_2}^{p_1} k\,dp\,dA, \tag{2}$$

where $k\equiv\frac{1}{2}(u^2+v^2)$, A is the computational area, $p_1(p_2)$ the pressure at the lower (higher) level and g the gravitational acceleration. Finally, the local rate of change of kinetic energy in a coordinate system centered with respect to the principal surface cyclone and anticyclone

becomes

$$\frac{\delta \mathrm{KE}}{\delta t}=\frac{1}{gA}\left[\int_A\int_{p_2}^{p_1}\frac{\partial k}{\partial t}dpdA+\int_A\int_{p_2}^{p_1}\nabla_p\cdot(k\bar{\mathbf{C}})dpdA+\int_A\int_{p_2}^{p_1}\frac{\partial k\omega_B}{\partial p}dpdA\right]$$

$$=-\frac{1}{gA}\int_A\int_{p_2}^{p_1}\nabla_p\cdot k\bar{\mathbf{V}}_h dpdA \tag{3a}$$

$$+\frac{1}{gA}\int_A\int_{p_2}^{p_1}\nabla_p\cdot k\bar{\mathbf{C}}dpdA \tag{3b}$$

$$-\frac{1}{gA}\int_A\int_{p_2}^{p_1}\frac{\partial k\omega}{\partial p}dpdA \tag{3c}$$

$$+\frac{1}{gA}\int_A\int_{p_2}^{p_1}\frac{\partial k\omega_B}{\partial p}dpdA \tag{3d}$$

$$-\frac{1}{gA}\int_A\int_{p_2}^{p_1}\bar{\mathbf{V}}_h\cdot\nabla_p\Phi dpdA \tag{3e}$$

$$+D_r. \tag{3f}$$

Terms (3a) and (3c) represent the boundary fluxes through the horizontal and vertical walls of the moving system. The magnitude of these terms is an indication of the significance of the interaction between the system and its external environment. Terms (3b) and (3d) are the corresponding flux terms due to the motion of the system. Term (3e) is the generation term within the system due to cross-contour flow, while term (3f) is the overall dissipation per uuit area per unit time.

Subjective analyses of isogons, isotachs, heights and temperatures were prepared at 50 mb intervals for time periods 3–5. Numerous vertical cross sections were constructed in an effort to better resolve meteorological gradients. The final isogon, isotach and height analyses were then tabulated over a 13 by 13 computational grid for both the composite cyclone and anticyclone. The interpolated values were then filtered using a 25-point filter described by Bosart (1970) over the interior points to eliminate tabulation noise. A grid spacing of 254 km was employed, valid at 60°N on a polar stereographic map. The size of the computational array was chosen so as to encompass the entire region within the outermost closed surface isobar of the composite cyclone or anticyclone.

The kinematic method is then used to generate vertical velocities at 50 mb intervals from the subjectively determined u and v grid point values. These computed vertical velocities are then adjusted in turn by a procedure outlined by O'Brien (1970) in an effort to reduce the cumulative errors inherent to the kinematic method. At the lower boundary the procedure of Cressman (1960) is used to parameterize the effect of orography. Terrain heights were provided on magnetic tape by Mr. Roy Jenne of the National Center for Atmospheric Research. Likewise, the surface roughness procedure outlined by Lettau (1959) and used by Kung (1966a) is used to parameterize the effects of friction. The resulting vertical velocity and divergence profiles were then compared to the observed weather patterns using conventional and satellite data as a check on qualitative reasonableness.

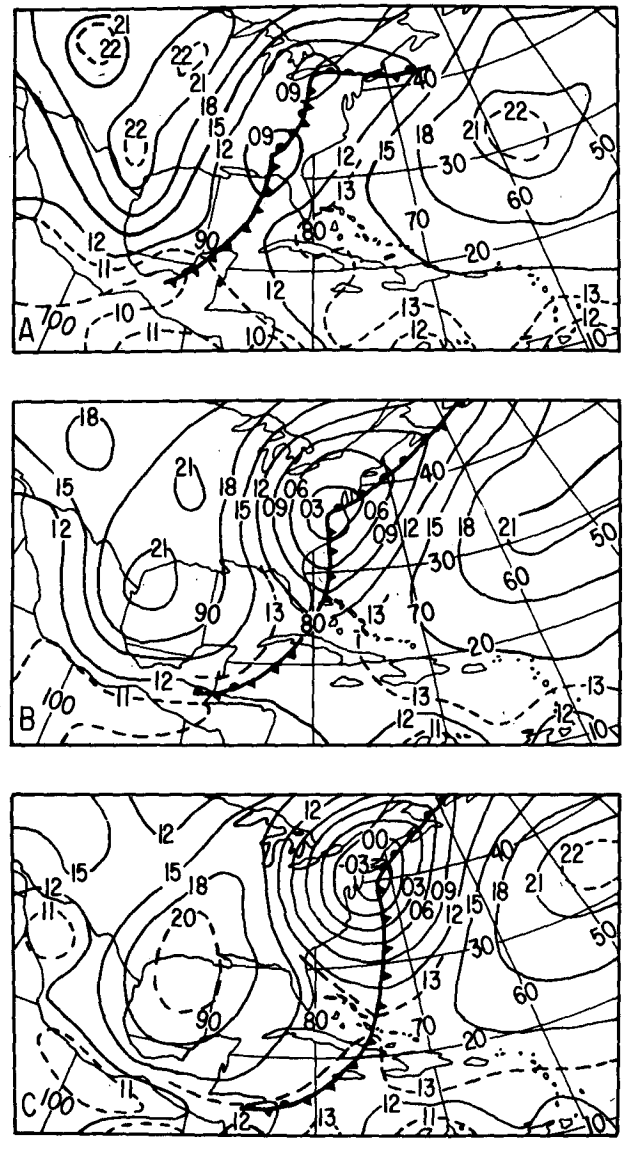

FIG. 1. Surface map (1000 mb) at time 3 (a), time 4 (b) and time 5 (c). Contour lines are drawn every 3 dam; dashed every 1 dam where necessary.

Simple centered finite differences are used to compute the various quantities on the right-hand side of Eq. (3). The local rate of change of the kinetic energy for the whole air column with respect to the moving system is taken as the difference of the total kinetic energy between the 12 h synoptic time periods. For physical consistency of the dynamical processes involved in the moving coordinate system, the quantities on the right-hand side of (3) are then averaged over the same two consecutive 12 h map times and then vertically integrated through the entire volume encompassing both the cyclone and anticyclone. The dissipation term (3f) is then computed as a residual by equating the difference between the left- and right-hand sides of (3). Errors inherent to the analysis and computation schemes are then contained in the residual term. McInnis and Kung (1972), for example, have used the residual technique, however, to extract meaningful information about atmospheric dissipation. Finally, the system vertical motion ω_B is computed as the difference of the grid-domain-averaged lower boundary condition over the same two consecutive map times.

5. Synoptic situation

At the outset of our composite case study a polar anticyclone with a closed 240 m center was located over Montana. This anticyclone moved rapidly southeastward across Wyoming and Colorado and was located over Texas at time period 3 (see Fig. 1a). The surface center continued to move southeastward over the next 12 h before eventually turning eastward and then northeastward (Figs. 1b, 1c). The main cyclone developed on a trailing polar front which was located over the southern United States at time periods 1 and 2. Cyclogenesis began at time period 3 over Georgia (Fig. 1a). This cyclone then moved northeastward for the next 24 h while maintaining a deepening rate of 60 m (12 h)$^{-1}$ (Figs. 1b, 1c). Little additional deepening was observed after time period 5.

At 500 mb the main trough was located to the lee of the Rockies at time period 1 (not shown). The 500 mb thermal trough was displaced upstream of the height trough at this time, indicative of an intensifying system. The 500 mb height trough moved eastward at 15 m s^{-1}, while continuing to intensify and was situated over the Great Plains and the Gulf of Mexico at time period 3 (Fig. 2a). This trough moved eastward at about the same speed for the next 24 h, while slowly overtaking the surface cyclone as cyclogenesis took place (Figs. 2b, 2c). In many respects the composite synoptic situation is similar to the case study described by Newton and Palmen (1963).

The moving computation domains for the composite cyclone-anticyclone couplet are shown in Fig. 3. The surface position of the cyclone and anticyclone is indicated by the letters L and H, while the numerical prefix indicates the time period.

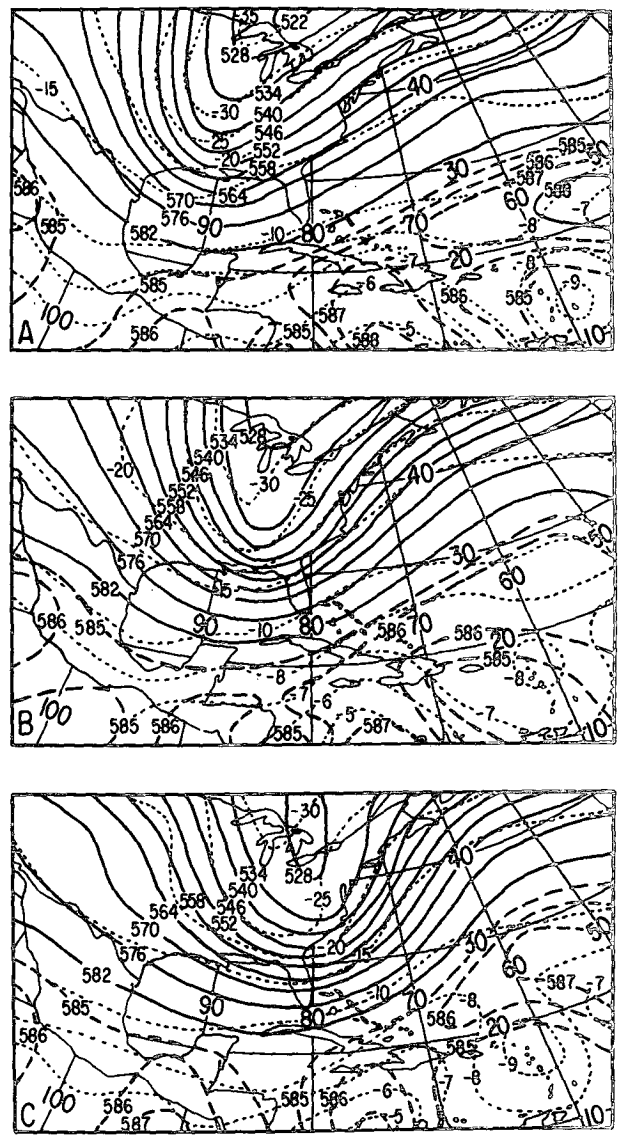

FIG. 2. 500 mb map at time 3 (a), time 4 (b) and time 5 (c). Contour lines are drawn every 6 dam; dashed every 3 (or 1) dam where necessary. Dotted lines are isotherms at 5°C intervals; at 6°C (or 1°C) intervals where necessary.

6. Results

a. *Anticyclone region*

Tables 1 and 2 and Fig. 4 depict the solution of Eq. (3) for the composite anticyclone region for time periods 3–4 and 4–5. Generation or destruction of kinetic energy due to the horizontal flux of kinetic energy and cross-contour flow are the dominant budget terms throughout both periods. Coincident with the onset of cyclogenesis after time period 3, an export of kinetic energy from the anticyclone region is seen from all pressure layers with a maximum in the 250–200 mb region. Significant destruction of kinetic energy by

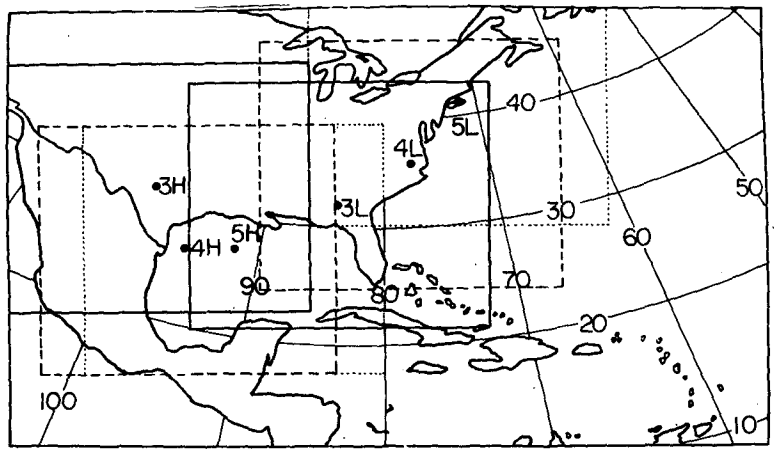

FIG. 3. Limited region moving with the surface anticyclone (H) and cyclone (L). Solid, dashed and dotted lines are boundaries at times 3, 4 and 5, respectively.

cross-contour flow is noted above 300 mb accompanied by modest generation in the 650–300 mb layer. Likewise, cross-contour generation of kinetic energy is noted from 1000–850 mb with weak destruction in the 850–650 mb layer. The horizontal system flux of kinetic energy acts as a sink in the 600–300 mb layer and a

TABLE 1. Kinetic energy budget terms [see Eq. (3)] averaged over the computation domain (11×11 grid) for different pressure layers over the surface anticyclone from time 3 to time 4. Units are W m^{-2}. Computed error bounds are in parentheses (see text).

Layer (mb)	$\frac{\delta KE}{\delta t}$	$-\frac{1}{gA}\int_A\int_{p_2}^{p_1}\nabla_p \cdot k\overline{V}_h dpdA$	$+\frac{1}{gA}\int_A\int_{p_2}^{p_1}\nabla_p \cdot k\overline{C}dpdA$	$-\frac{1}{gA}\int_A\int_{p_2}^{p_1}\frac{\partial k\omega}{\partial p}dpdA$	$-\frac{1}{gA}\int_A\int_{p_2}^{p_1}\overline{V}_h \cdot \nabla_p\Phi dpdA$	D_r
150–100	−0.10	−2.58	0.23	−0.87	−5.15	8.26
	(0.19)	(0.55)	(0.14)	(0.31)	(0.66)	(0.94)
200–150	0.13	−5.42	0.31	−1.53	−4.35	11.13
	(0.27)	(1.24)	(0.20)	(0.55)	(0.82)	(1.62)
250–200	0.61	−7.14	0.31	−0.52	−2.24	10.20
	(0.31)	(1.55)	(0.23)	(0.59)	(0.81)	(1.89)
300–250	0.28	−6.15	0.05	−0.31	−2.93	9.62
	(0.31)	(1.58)	(0.23)	(0.55)	(0.73)	(1.86)
350–300	−0.04	−4.16	−0.13	−0.39	0.65	3.99
	(0.30)	(1.44)	(0.22)	(0.55)	(0.62)	(1.71)
400–350	−0.08	−2.82	−0.14	−0.35	1.79	1.43
	(0.22)	(0.95)	(0.15)	(0.41)	(0.45)	(1.16)
450–400	−0.10	−2.20	−0.12	0.07	1.54	0.62
	(0.15)	(0.57)	(0.10)	(0.26)	(0.33)	(0.74)
500–450	−0.19	−1.66	−0.15	0.19	0.87	0.56
	(0.10)	(0.36)	(0.07)	(0.18)	(0.24)	(0.48)
550–500	−0.36	−1.26	−0.17	0.70	−0.36	0.76
	(0.08)	(0.27)	(0.06)	(0.13)	(0.18)	(0.36)
600–550	−0.53	−0.92	−0.14	0.33	0.93	−0.74
	(0.07)	(0.20)	(0.05)	(0.11)	(0.15)	(0.28)
650–600	−0.42	−0.81	−0.07	0.50	0.26	−0.31
	(0.06)	(0.16)	(0.04)	(0.08)	(0.11)	(0.22)
700–650	−0.20	−0.74	0.01	0.59	−1.72	0.65
	(0.06)	(0.12)	(0.03)	(0.07)	(0.09)	(0.18)
750–700	−0.03	−0.56	0.06	0.67	−0.66	0.45
	(0.05)	(0.09)	(0.03)	(0.05)	(0.07)	(0.14)
800–750	0.06	−0.32	0.07	0.34	0.03	−0.06
	(0.04)	(0.06)	(0.02)	(0.03)	(0.06)	(0.10)
850–800	0.07	−0.18	0.11	0.29	0.15	0.01
	(0.03)	(0.04)	(0.01)	(0.02)	(0.04)	(0.07)
1000–850	0.15	−0.24	0.37	0.25	0.98	−1.20
	(0.02)	(0.02)	(0.01)	(0.01)	(0.03)	(0.04)
Total	−0.75	−37.15	0.61	−0.06	−9.52	45.37
	(0.70)	(3.21)	(0.51)	(1.30)	(1.77)	(3.99)

TABLE 2. As in Table 1 except from time 4 to time 5.

Layer (mb)	$\frac{\delta KE}{\delta t}$	$-\frac{1}{gA}\int_A\int_{p_2}^{p_1}\nabla_p \cdot k\overline{V}_h dpdA$	$+\frac{1}{gA}\int_A\int_{p_2}^{p_1}\nabla_p \cdot k\overline{C}dpdA$	$-\frac{1}{gA}\int_A\int_{p_2}^{p_1}\frac{\partial k\omega}{\partial p}dpdA$	$-\frac{1}{gA}\int_A\int_{p_2}^{p_1}\overline{V}_h \cdot \nabla_p\Phi dpdA$	D_r
150–100	0.44	−2.83	0.89	−0.94	−3.75	7.08
	(0.19)	(0.58)	(0.08)	(0.31)	(0.67)	(0.96)
200–150	0.35	−6.66	1.55	1.36	−2.53	9.36
	(0.27)	(1.22)	(0.12)	(0.52)	(0.81)	(1.58)
250–200	−0.10	−9.90	1.95	−0.02	−1.88	9.74
	(0.31)	(1.59)	(0.13)	(0.59)	(0.81)	(1.91)
300–250	−0.12	−9.46	1.93	0.26	−3.10	10.25
	(0.31)	(1.54)	(0.13)	(0.52)	(0.72)	(1.82)
350–300	−0.03	−6.69	1.63	−0.32	1.21	4.14
	(0.30)	(1.40)	(0.12)	(0.53)	(0.61)	(1.65)
400–350	−0.17	−4.80	1.33	−0.41	2.47	1.24
	(0.22)	(0.90)	(0.09)	(0.40)	(0.44)	(1.10)
450–400	−0.19	−3.86	1.14	−0.01	1.09	1.45
	(0.15)	(0.54)	(0.06)	(0.24)	(0.33)	(0.70)
500–450	−0.17	−2.72	0.95	−0.02	0.37	1.25
	(0.10)	(0.34)	(0.04)	(0.16)	(0.23)	(0.45)
550–500	−0.12	−2.03	0.82	0.28	−0.35	1.16
	(0.08)	(0.24)	(0.03)	(0.12)	(0.17)	(0.33)
600–550	−0.02	−1.57	0.71	0.24	0.93	−0.33
	(0.07)	(0.18)	(0.03)	(0.10)	(0.14)	(0.26)
650–600	−0.01	−1.28	0.62	0.33	0.45	−0.13
	(0.06)	(0.14)	(0.02)	(0.08)	(0.11)	(0.20)
700–650	−0.07	−1.01	0.52	0.50	0.60	0.52
	(0.06)	(0.11)	(0.02)	(0.06)	(0.09)	(0.16)
750–700	−0.08	−0.78	0.43	0.45	−0.62	0.44
	(0.05)	(0.08)	(0.02)	(0.05)	(0.07)	(0.13)
800–750	−0.09	−0.57	0.34	0.40	−0.04	−0.22
	(0.04)	(0.05)	(0.01)	(0.03)	(0.06)	(0.09)
850–800	−0.13	−0.37	0.25	0.36	−0.33	−0.03
	(0.03)	(0.04)	(0.01)	(0.02)	(0.04)	(0.07)
1000–850	−0.35	−0.43	0.29	0.22	0.67	−1.10
	(0.02)	(0.02)	(0.00)	(0.01)	(0.03)	(0.04)
Total	−0.84	−54.95	15.34	−0.03	−6.01	44.82
	(0.70)	(3.16)	(0.29)	(1.25)	(1.76)	(3.90

source elsewhere, while the vertical flux is a source below 400 mb and a sink otherwise. Finally, the dissipation term computed as a residual proved, rather surprisingly, to be a rather large source of kinetic energy in the upper troposphere.

From time 4 to time 5 the horizontal export of kinetic energy increases by 20–30% in the upper troposphere. During this period major cyclogenesis continues downstream, while polar air between the cyclone and anticyclone reaches its southernmost extent. Cross-contour generation and destruction of kinetic energy continues as in the previous period but reduced in magnitude by 20–30%. During time 4 to time 5 the belt of strongest winds in the upper troposphere moves out of the northwesterly flow computational region and becomes embedded in the southwesterly region ahead of the downstream trough axis. The vertical flux of kinetic energy exhibits a similar profile as previously except that the transition level lowers to 500 mb. In addition, the horizontal system flux takes on added importance as a source of kinetic energy in the mid and upper troposphere. Finally, the residual dissipation term continues to be a major source of kinetic energy, especially in the upper troposphere.

b. Cyclone region

Tables 3 and 4 and Fig. 5 present the corresponding kinetic energy budget results for the cyclone region from times 3–4 and times 4–5. From time 3 to time 4, as cyclogenesis is initiated, the cross-contour generation term represents the most important mechanism. It exhibits a double-maxima structure with a major peak in the 300–350 mb layer near the jet stream and a secondary maximum in the lower troposphere. The remaining terms also contribute significantly to the kinetic energy balance. The horizontal system flux tends to decrease the total kinetic energy of the system, while the larger horizontal flux tends to advect the existing kinetic energy from the upstream anticyclone area. The vertical flux has a profile opposite in sign but larger in magnitude to the corresponding anticyclone case. It transports kinetic energy from the mid and lower

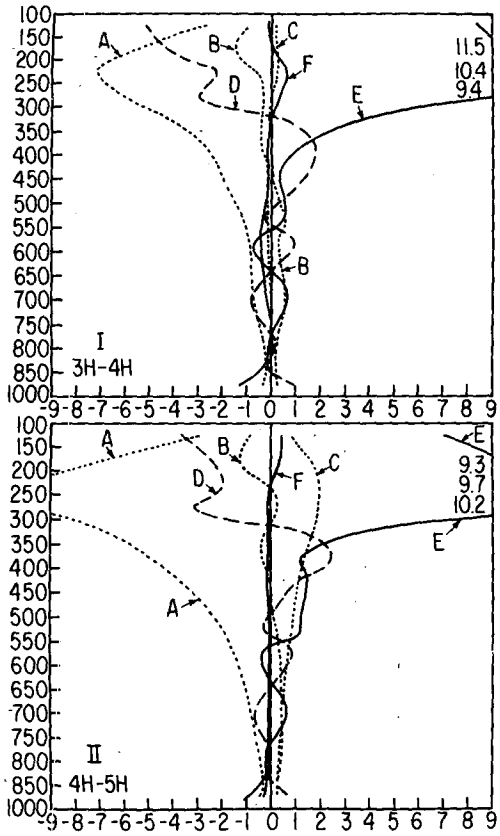

FIG. 4. Vertical profiles of kinetic energy budget terms in W m^{-2}: (A) horizontal flux; (B) vertical flux; (C) horizontal system flux; (D) vertical system flux; (E) cross-contour term; (F) residual term; and (G) local accumulation for the surface anticyclone from time 3 to time 4 (I) and time 4 to time 5 (II).

troposphere upward into the jet stream region. As in the anticyclone case the residual dissipation term is dominant with a sharp peak contributing to destruction of kinetic energy near the jet stream level and in the 1000–850 mb layer.

From time 4 to time 5 the results are similar to those of the previous period except that the magnitudes of the individual terms are generally larger, consistent with the intensification of cyclogenesis. Note that surface cyclone intensification is reflected as a net accumulation of kinetic energy for the air column below 350 mb from time 3 to time 4 and below 800 mb from time 4 to time 5. Cross-contour generation of kinetic energy increases significantly in the latter period, especially in the upper troposphere, and dominates the horizontal influx. This suggests that after the initiation of cyclogenesis, generation of kinetic energy within the moving storm volume is more important than advection of preexisting kinetic energy in maintaining storm intensity against friction dissipation. Finally, the system dissipation computed as a residual contributes substantially to destruction of kinetic energy, especially in the upper troposphere and in the second time period.

7. Discussion

In a quasi-Lagrangian framework our results suggest that anticyclone regions play a major role as exporters of kinetic energy to downstream cyclogenetic areas. From time 3 to time 4 a surface to 100 mb average of 37.2 W m^{-2} is exported out of the anticyclone region compared to 9.5 W m^{-2} which is dissipated within the region due to the cross-contour flow mechanism. The export increases to 55.0 W m^{-2} while the cross-contour dissipation reduces to 6.0 W m^{-2} in the following 12 h time period. The vertically averaged horizontal system flux ranges from an insignificant 0.6 W m^{-2} to 15.3 W m^{-2} for these time periods, respectively. Export of kinetic energy from the anticyclone region is most pronounced in the upper troposphere. Inspection of the composite case contour maps discloses that a speed maximum initially embedded in the upper tropospheric northwesterly flow migrates through the downstream trough axis during the 24 h period in question as cyclogenesis begins downstream.

Somewhat different behavior is observed for the cyclone region as the generation of kinetic energy by cross-contour flow from the surface to 100 mb increases from 24.5 to 64.6 W m^{-2} from time 3 to time 4 and time 4 to time 5, respectively. Meanwhile, the vertically

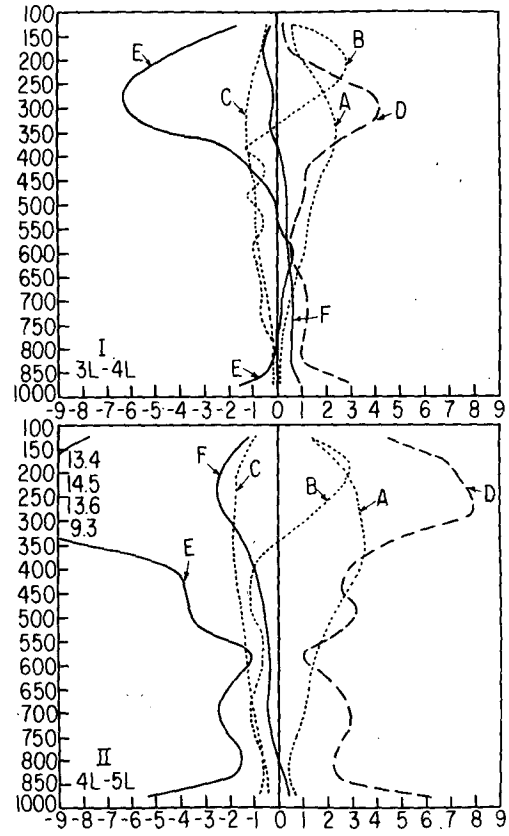

FIG. 5. As in Fig. 4 except for the surface cyclone from time 3 to time 4 (I) and from time 4 to time 5 (II).

TABLE 3. As in Table 1 except over the surface cyclone from time 3 to time 4.

Layer (mb)	$\frac{\delta KE}{\delta t}$	$-\frac{1}{gA}\int_A\int_{p_2}^{p_1}\nabla_p \cdot k\bar{V}_h dp dA$	$+\frac{1}{gA}\int_A\int_{p_2}^{p_1}\nabla_p \cdot k\bar{C} dp dA$	$-\frac{1}{gA}\int_A\int_{p_2}^{p_1}\frac{\partial k\omega}{\partial p} dp dA$	$-\frac{1}{gA}\int_A\int_{p_2}^{p_1}\bar{V}_h \cdot \nabla_p\Phi dp dA$	D_r
150–100	−0.33	0.66	−0.46	0.68	0.23	−1.43
	(0.19)	(0.70)	(0.21)	(0.40)	(0.75)	(1.14)
200–150	−0.66	0.79	−0.67	2.57	0.39	−3.74
	(0.27)	(1.62)	(0.32)	(0.69)	(0.96)	(2.05)
250–200	−0.39	1.42	−0.94	2.72	2.03	−5.62
	(0.31)	(2.17)	(0.37)	(0.79)	(0.97)	(2.55)
300–250	−0.15	1.83	−1.19	1.61	3.94	−6.34
	(0.31)	(2.26)	(0.38)	(0.75)	(0.90)	(2.59)
350–300	−0.31	2.23	−1.23	0.12	4.12	−5.55
	(0.30)	(2.09)	(0.37)	(0.77)	(0.77)	(2.40)
400–350	0.08	2.42	−1.19	−1.28	2.29	−2.15
	(0.22)	(1.35)	(0.26)	(0.56)	(0.55)	(1.60)
450–400	0.34	2.01	−1.09	−0.50	1.20	−1.29
	(0.15)	(0.80)	(0.17)	(0.36)	(0.41)	(1.00)
500–450	0.36	1.53	−0.97	−1.23	1.10	−0.08
	(0.10)	(0.52)	(0.12)	(0.24)	(0.30)	(0.67)
550–500	0.39	1.28	−0.93	−0.61	0.72	−0.07
	(0.08)	(0.38)	(0.10)	(0.18)	(0.22)	(0.49)
600–550	0.42	1.20	−0.84	−0.97	0.50	0.52
	(0 07)	(0.30)	(0.08)	(0.15)	(0.19)	(0.40)
650–600	0.53	0.96	−0.72)	−0.88	0.74	0.43
	(0.06)	(0.24)	(0.07)	(0.12)	(0.15)	(0.33)
700–650	0.66	0.64	−0.55	−0.65	1.10	0.12
	(0.06)	(0.20)	(0.06)	(0.10)	(0.13)	(0.27)
750–700	0.65	0.35	−0.36	−0.71	1.22	0.14
	(0.05)	(0.16)	(0.05)	(0.08)	(0.10)	(0.22)
800–750	0.60	0.17	−0.25	−0.32	1.07	−0.07
	(0.04)	(0.10)	(0.04)	(0.05)	(0.08)	(0.14)
850–800	0.55	0.08	−0.19	−0.17	0.93	−0.11
	(0.03)	(0.06)	(0.03)	(0.03)	(0.06)	(0.10)
1000–850	0.96	0.11	−0.26	−0.11	2.87	−1.64
	(0.02)	(0.03)	(0.01)	(0.01)	(0.04)	(0.05)
Total	3.71	17.67	−11.84	0.29	24.45	−26.88
	(0.70)	(4.52)	(0.84)	(1.74)	(2.13)	(5.40)

averaged horizontal inflow of kinetic energy into the moving cyclone region is 17.7 and 32.2 W m^{-2} for the same periods, while the horizontal system flux provides a loss of kinetic energy of 11.8 and 20.2 W m^{-2}, respectively. In summary we find that cyclone initiation and ensuing development are accompanied by large kinetic energy generation within the cyclone region due to the cross-contour flow mechanism. The horizontal import of kinetic energy into the region is also significant but secondary. The reverse appears to be true during the same time periods in the upstream anticyclone region as the horizontal export of kinetic energy dominates the cross-contour mechanism.

The dissipation term computed as a residual contributes toward a rather large vertically averaged generation of kinetic energy of 45.4 and 44.8 W m^{-2}, respectively, in the anticyclone region over both 12 h periods. Destruction of kinetic energy amounts to 26.9 and 91.3 W m^{-2}, respectively, by the residual term for the cyclone region over these same time periods. Generation of kinetic energy by the dissipation term when computed as a residual has been reported by other investigators from both long-term averaged data (e.g., Holopainen, 1963; Kung, 1966a, b, 1967, 1969, 1970; Smith, 1973a; and Kung and Baker, 1975) as well as individual case studies (e.g., Smith, 1973b, c; Vincent *et al.*, 1974).

It is important to remember that dissipation computed as a residual includes many effects besides frictional dissipation in addition to overall computational errors. Subsynoptic-scale grid processes not resolvable with the operational radiosonde network probably provide a source of kinetic energy in the mid and upper troposphere of the anticyclone environment. Some support for this is provided by McInnis and Kung (1972) and Kung and Tsui (1975). It is also possible that energy generation or relative boundary kinetic energy transport due to quasi-horizontal motions corresponding to wavenumbers representing smaller synoptic-scale wavenumbers, which are not actually subgrid scale, are underestimated due to limited data density and the use of filters. Finally, the effect of the energy exchange between the planetary-scale waves and the synoptic-scale waves is unknown because the former

TABLE 4. As in Table 1 except over the surface cyclone from time 4 to time 5.

Layer (mb)	$\frac{\delta KE}{\delta t}$	$-\frac{1}{gA}\int_A\int_{p_2}^{p_1}\nabla_p \cdot k\bar{\mathbf{V}}_h dpdA$	$+\frac{1}{gA}\int_A\int_{p_2}^{p_1}\nabla_p \cdot k\bar{\mathbf{C}} dpdA$	$-\frac{1}{gA}\int_A\int_{p_2}^{p_1}\frac{\partial k\omega}{\partial p}dpdA$	$-\frac{1}{gA}\int_A\int_{p_2}^{p_1}\bar{\mathbf{V}}_h \cdot \nabla_p\Phi\, dpdA$	D_r
150–100	−1.17	1.39	−0.96	1.33	4.58	−7.51
	(0.19)	(0.64)	(0.18)	(0.37)	(0.72)	(1.07)
200–150	−2.04	2.55	−1.54	2.98	6.93	−12.97
	(0.27)	(1.44)	(0.27)	(0.61)	(0.90)	(1.85)
250–200	−2.52	3.12	−1.69	2.72	7.54	−14.21
	(0.31)	(1.90)	(0.31)	(0.71)	(0.90)	(2.26)
300–250	−2.30	3.32	−1.74	1.67	8.03	−13.59
	(0.31)	(2.03)	(0.31)	(0.73)	(0.84)	(2.36)
350–300	−1.66	3.61	−1.82	.42	5.66	−9.53
	(0.30)	(1.88)	(0.30)	(0.74)	(0.72)	(2.19)
400–350	−1.19	3.55	−1.75	−0.77	3.33	−5.55
	(0.22)	(1.24)	(0.21)	(0.55)	(0.52)	(1.48)
450–400	−0.94	3.06	−1.65	−1.03	2.69	−4.02
	(0.15)	(0.77)	(0.14)	(0.35)	(0.39)	(0.96)
500–450	−0.75	2.51	−1.48	−1.13	3.19	−3.85
	(0.10)	(0.49)	(0.10)	(0.24)	(0.28)	(0.63)
550–500	−0.54	2.08	−1.38	−0.70	2.73	−3.28
	(0.08)	(0.37)	(0.08)	(0.18)	(0.21)	(0.48)
600–550	−0.43	1.61	−1.28	−0.65	1.05	−1.16
	(0.07)	(0.30)	(0.07)	(0.15)	(0.18)	(0.39)
650–600	−0.33	1.32	−1.11	−0.70	2.02	−1.86
	(0.06)	(0.25)	(0.06)	(0.13)	(0.15)	(0.33)
700–650	−0.50	1.23	−1.03	−1.08	2.87	−2.48
	(0.06)	(0.20)	(0.05)	(0.10)	(0.13)	(0.27)
750–700	−0.36	1.00	−0.86	−1.05	2.96	−2.41
	(0.05)	(0.17)	(0.05)	(0.09)	(0.11)	(0.23)
800–750	−0.02	0.63	−0.63	−0.71	2.32	−1.64
	(0.04)	(0.11)	(0.03)	(0.06)	(0.08)	(0.16)
850–800	0.09	0.47	−0.51	−0.49	2.33	−1.72
	(0.03)	(0.07)	(0.02)	(0.03)	(0.07)	(0.11)
1000–850	0.37	0.72	−0.76	−0.43	6.32	−5.49
	(0.02)	(0.04)	(0.01)	(0.02)	(0.04)	(0.06)
Total	−14.29	32.19	−20.18	0.40	64.57	−91.27
	(0.70)	(4.07)	(0.70)	(1.63)	(2.00)	(4.92)

TABLE 5. Published computations of kinetic energy generation and residual term contributions to the kinetic energy budgets. Units in W m^{-2}.

Author	Data	Layer	$-\frac{1}{gA}\int_A\int_{p_2}^{p_1}\bar{\mathbf{V}}_h \cdot \nabla_p\Phi dpdA$	D_r
Smith (1973b)	Mature cyclone	Surface to 200 mb	10.0	−15.5
	Cyclone vicinity (three days)	—	18.2	−38.4
	Anticyclone vicinity	—	0.4	0.0
McInnis and Kung (1972)	Thunderstorm area (nine case average)	Surface to 100 mb	23.8	−26.1
Kung (1969)	Three winter months (cyclone and anticyclone)	Surface to 50 mb	17.5	−8.7
Kung and Baker (1975)	Cyclone North America: five years	Surface to 100 mb	8.5	−6.3
	Anticyclone North America: five years	Surface to 100 mb	−1.8	2.7
Present study	High (time 3–4)	Surface to 100 mb	−9.5	45.3
	High (time 4–5)	—	−6.0	44.8
	Low (time 3–4)	—	24.5	−26.8
	Low (time 4–5)	—	64.6	−91.2
	Average (low and high)	—	18.4	−7.0

TABLE 6. Horizontal flux (top lines), cross-contour generation (middle lines) and residual (bottom lines) terms for anticyclone and cyclone from time 3 to 5, integrated over different grid areas. Units in W m^{-2}. Parentheses denote the value decreases as the area decreases.

	Time period	Grid area 11×11	9×9	7×7	5×5	3×3
Anticyclone						
Time 3–4	$-\frac{1}{gA}\int_A\int_{p_2}^{p_1}\nabla_p\cdot k\bar{\mathbf{V}}_h dp dA$	−37.2	−42.1	−53.7	−63.8	−71.9
	$-\frac{1}{gA}\int_A\int_{p_2}^{p_1}\bar{\mathbf{V}}_h\cdot\nabla_p\Phi dp dA$	−9.5	−10.8	−12.7	−19.8	−28.5
	D_r	45.3	49.8	60.0	70.8	80.9
Time 4–5	$-\frac{1}{gA}\int_A\int_{p_2}^{p_1}\nabla_p\cdot k\bar{\mathbf{V}}_h dp dA$	−55.0	−65.7	−87.3	−93.2	(−81.1)
	$-\frac{1}{gA}\int_A\int_{p_2}^{p_1}\bar{\mathbf{V}}_h\cdot\nabla_p\Phi dp dA$	−6.0	−8.9	−19.1	−35.0	−47.5
	D_r	44.8	55.6	80.5	96.3	(94.6)
Cyclone						
Time 3–4	$-\frac{1}{gA}\int_A\int_{p_2}^{p_1}\nabla_p\cdot k\bar{\mathbf{V}}_h dp dA$	17.7	23.8	32.5	(19.3)	(−11.6)
	$-\frac{1}{gA}\int_A\int_{p_2}^{p_1}\bar{\mathbf{V}}_h\cdot\nabla_p\Phi dp dA$	24.5	26.0	33.3	47.9	60.6
	D_r	−26.8	−32.1	−46.5	−54.8	(−44.4)
Time 4–5	$-\frac{1}{gA}\int_A\int_{p_2}^{p_1}\nabla_p\cdot k\bar{\mathbf{V}}_h dp dA$	32.2	39.7	53.6	62.3	89.8
	$-\frac{1}{gA}\int_A\int_{p_2}^{p_1}\bar{\mathbf{V}}_h\cdot\nabla_p\Phi dp dA$	64.6	66.9	74.7	86.5	92.0
	D_r	−91.2	−102.6	−130.3	−164.4	−208.5

are incapable of being resolved within the limited area computational domain.

In an effort to assess the quantitative reasonableness of our results comparison is made in Table 5 to some of the published findings of other researchers for both time averaged and individual case studies. Only the dissipation and cross-contour terms are included. Some caution is required in the interpretation of the results, however, in that the other investigations were conducted in Eulerian coordinate systems. Likewise, differences would be expected on the basis of differing synoptic characteristics of the individual case studies. Recall that the composite used in the present study is generated from four relatively intense cyclone-anticyclone couplets during the North American winter season. Thus our computed results should be considerably larger than corresponding values derived from long-term time-averaged data. As significant cyclogenesis was initiated from time 3 to time 4, our results are comparable to those of Smith (1973b) for a three-day average in a cyclone environment as well as McInnis and Kung (1972) for a thunderstorm environment. From time 4 to time 5, however, our results are markedly larger than those from any of the other tabulated papers. The overall kinetic energy change due to cross-isobar flow and dissipation when vertically averaged for both cyclone and anticyclone is comparable to Kung's (1969) results derived from a three-month winter season.

The total magnitudes of the three major vertically integrated terms in the kinetic energy budget (i.e., horizontal flux, generation and residual terms) are presented in Table 6 to show their variation with respect to a change in grid domain size. In general the magnitudes increase as the domain area decreases with a few exceptions for a 3 by 3 grid size. The same was true when individual pressure layer contributions were considered as a function of grid size (not shown). The consistency of this variation for both the individual pressure layers and the total air column over different grid domains strengthens the validity of the results of this study. Additionally, terms (3a) and (3e) in the kinetic energy budget equation were computed as $k\nabla_p\cdot\bar{\mathbf{V}}_h+\bar{\mathbf{V}}_h\cdot\nabla_p k$ and $\nabla_p\cdot\Phi\bar{\mathbf{V}}_h-\Phi\nabla_p\cdot\bar{\mathbf{V}}_h$, respectively. The results showed that the differences between the two computational modes were much less than 1% for all pressure layers.

As a further check, frictional dissipation computed from the Lettau (1959) model for the surface to 800 mb layer is compared with dissipation computed by the

TABLE 7. Comparison of frictional dissipation (W m^{-2}) as derived from the Lettau (1959) model versus computed dissipation as a residual. Values of V_{gs} (m s^{-1}), C_{gs} (10^{-3}) and α_0 (deg) are surface geostrophic wind, surface geostrophic drag coefficient and angle formed by surface stress and the surface geostrophic wind, respectively.

Time period		V_{gs}	C_{gs}	α_0	Frictional dissipation	
					Model	Residual
Anticyclone	3	11.5	35.7	24.5	3.7	1.2 (anticyclone: time 3–4)
	4	13.7	34.5	23.6	6.0	1.1 (anticyclone: time 4–5)
	5	11.6	34.8	23.8	5.2	
	Average	12.3	35.0	24.0	4.7	1.2
Cyclone	3	9.2	34.7	23.7	2.0	1.8 (cyclone: time 3–4)
	4	13.0	33.2	22.7	3.9	7.2 (cyclone: time 4–5)
	5	14.5	34.0	23.2	5.5	
	Average	12.2	34.0	23.2	3.8	4.5
Cyclone-anticyclone	Average	12.3	34.5	23.6	4.3	2.9

residual techniques for the same pressure layer in Table 7. Agreement between the two methods is only fair with the residual technique providing an underestimate in the anticyclone region and an overestimate for the last time period for the cyclone domain. The residual average of 2.9 W m^{-2} is comparable to Kung's (1969) estimate of 3.2 W m^{-2} for six months of winter-averaged data. Likewise, the value of 7.2 W m^{-2} from time 4 to time 5 in the cyclone domain is comparable to the 8.4 W m^{-2} reported by Smith (1973b) for a mature cyclone and the 7.1 W m^{-2} computed by Gall and Johnson (1971) using the Lettau (1959) model on a storm system of similar magnitude and intensity. Overall, however, there appears to be reasonable agreement between the computed findings of the present investigation and results presented previously.

8. Error analysis

This section attempts to assess the possible influence of observational and computational errors on the overall results. These errors may be partly random and partly systematic (e.g., Kurihara, 1961; Hodge and Harmantas, 1965; Holopainen, 1973). Kurihara's (1961) error criteria for wind speed and geopotential heights were linearly interpolated to 50 mb vertical intervals. If X is the random error, the standard error of the mean value of X for N cases will be $X/N^{\frac{1}{2}}$ (Kurihara, 1961). Similarly, the random uncertainties in the resulting mean value are reduced and are inversely proportional to the square root of the number of grids, with the value averaged over the grid points. Furthermore, if we assume that the errors involved in different terms in the budget equations are independent of each other (i.e., uncorrelated), the standard error of the residual term can be computed as

$$\Delta X=(\sum_i \Delta X_i^2)^{\frac{1}{2}}, \tag{4}$$

where ΔX_i is the standard error associated with the ith term in the budget equation (Holopainen, 1973). For the record it should be noted that the data used to derive the various terms in Eq. (3) are not independent in that data for some of the grid points are used in the computation of two or more terms. Thus, covariances are present and the computed error bounds are probably then underestimates.

Kurihara's empirical results showed that the errors in the wind observations are mainly random, especially at higher levels. The randomness of errors on the different terms in the kinetic energy budget equation is assumed throughout the computation, even though the total errors in the observational parameters were used. For example, the error in the horizontal flux of kinetic energy was computed as

$$\Delta\left|\frac{1}{gA}\int_A\int_{p_2}^{p_1}(\nabla_p\cdot\tfrac{1}{2}\mathbf{V}_h^2\bar{\mathbf{V}}_h)dpdA\right|$$

$$=\frac{1}{gA}\int_A\int_{p_2}^{p_1}\left[\tfrac{1}{2}\mathbf{V}_h^2\Delta|\nabla_p\cdot\bar{\mathbf{V}}_h|+|\nabla_p\cdot\bar{\mathbf{V}}_h||\mathbf{V}_h||\Delta\mathbf{V}_h|\right.$$

$$\left.+\frac{2}{\sqrt{2}}\left(\left|\frac{\partial\tfrac{1}{2}\mathbf{V}_h^2}{\partial x}\right||\Delta\mathbf{V}_h|+|\mathbf{V}_h|\left|\frac{\partial(|\mathbf{V}_h||\Delta\mathbf{V}_h|)}{\partial x}\right|\right)\right]dpdA, \tag{5}$$

where Δ indicates the error. Since an adjustment technique was used in the computation of the divergence and vertical velocity, it is difficult to assess the errors in these adjusted values. Arbitrarily, it is assumed that error $|\Delta\nabla\cdot\bar{\mathbf{V}}_h|$ is comparable to the error of $|\Delta\zeta|$ and thus the error $|\Delta\omega|$ is computed through the integration of the continuity equation.

The errors for each term in the kinetic energy equation are included in Tables 1–4. In general, the errors in the horizontal flux term and the residual term are the largest, while the errors in the local accumulation and system flux terms are the smallest among all the terms at all levels for both the cyclone and the anticyclone cases. Comparing the values presented in Tables 1–4 with the errors of the different terms, we find that the

major terms are more reliable than the minor terms at all levels. Note that the residual term is generally reliable in both sign and magnitude. While the residual term is most reliable at all levels for surface cyclone from time 4 to time 5, it has an error larger than the term itself in the layer 850–800 mb for the other situations and in the layer 550–450 mb from time 3 to time 4 for the surface cyclone due to the smallness of the term (see also Figs. 4 and 5).

9. Conclusions

A composite quasi-Lagrangian kinetic energy budget is constructed from four synoptically similar cases of polar air penetration into the Caribbean from off the North American continent. Computations were carried out for both the upstream anticyclone and downstream cyclone accompanying the polar outbreak.

Use of the residual technique suggests an average upscale energy exchange of 45.0 W m^{-2} over the anticyclone volume with a corresponding downscale energy transfer of 59.0 W m^{-2} over the cyclone volume for the 24 h period centered on the time of furthest southward cold air thrust as defined by the 1000–500 mb thickness patterns. The results also indicate that the verticul flux of kinetic energy ranges from 50 to 100% of the horizontal flux of kinetic energy and is of opposite sign below 400 mb in the cyclone volume. Furthermore, during incipient surface cyclogenesis the horizontal boundary flux of 17.7 W m^{-2} is a significant fraction of the local kinetic energy generation of 24.5 W m^{-2}, whereas in the following 12 h time period these numbers become 32.2 and 64.6 W m^{-2}, respectively. The corresponding figures for the anticyclone region include a horizontal export of kinetic energy of 37.2 and 55.0 W m^{-2} and local kinetic energy destruction of 9.5 and 6.0 W m^{-2}, respectively, for the same 12 h time periods.

While the current operational models in numerical weather prediction incorporate the frictional term through parameterization of classical energy dissipation in the boundary layer (e.g., Shuman and Hovermale, 1968), this study suggests that the frictional term may in some circumstances contribute to generation rather than dissipation under certain circumstances in the free atmosphere. More studies are needed from both observational and theoretical view points to better understand the interaction between synoptic-scale and mesoscale systems. Observational studies using a dense network (McInnis and Kung, 1972; Kung and Behrens, 1974) and using additional information from satellites (Wooldridge, 1972) are in line with this suggestion. In addition, this study further suggests that the composite method within a quasi-Lagrangian framework can be employed to better understand the pertinent dynamics of synoptic-scale systems.

Acknowledgments. The research reported here represents a portion of Dr. Chen's doctoral dissertation. Support was provided by National Science Foundation under Grant A023897002. The National Center for Atmospheric Research provided some of the data used in the calculations. The manuscript was typed by Ms. Sally Young and the figures drafted by Ms. Marilyn Peacock, Deborah Fondario, Andrew Fritz and David Palmiero aided in the data preparation. Our thanks to the referees for elucidating a number of errors and inconsistencies in the original text.

REFERENCES

Bosart L. F., 1970: Mid tropospheric frontogenesis. *Quart. J. Roy. Meteor. Soc.*, **96** 442–471.

Cressman, G. P. 1960: Improved terrain effects in barotropic forecasts. *Mon. Wea. Rev.*, **88**, 327–342.

Duquet, R. T., 1964: Data processing for isentropic analysis. Tech. Rep. No. 1, Contract AF(30-1) 3317, The Pennsylvania State University, 18 pp.

Dutton, J. A., and D. R. Johnson, 1967: The theory of available potential energy and a variational approach to atmospheric energetics. *Advances in Geophysics*, Vol. 12, Academic Press, 333–436.

Gall, R. L., and D. R. Johnson, 1971: The generation of available potential energy of sensible heating: A case study. *Tellus*, **23**, 465–482.

Hodge, M. W., and C. Harmantas, 1965: Compatability of United States radiosondes. *Mon. Wea. Rev.*, **93**, 253–266.

Holopainen, E. O., 1963: On the dissipation of kinetic energy in the atmosphere. *Tellus*, **15**, 26–32.

——, 1973: An attempt to determine the effects of turbulent friction in the upper troposphere from the balance requirements of the large-scale flow: A frustrating experiment. *Geophysica*, **12**, 151–176.

Johnson, D. R., 1970: The available potential energy of storms. *J. Atmos. Sci.*, **27**, 727–741.

——, and W. K. Downey, 1975a: Azimuthally averaged transport and budget equations for storms: Quasi-Lagrangian diagnostics 1. *Mon. Wea. Rev.*, **103**, 967–979.

——, and ——, 1975b: The absolute angular momentum of storms: Quasi-Lagrangian diagnostics 2. *Mon. Wea. Rev.*, **103**, 1063–1076.

——, and ——, 1976: The absolute angular momentum budget of an extratropical cyclone: Quasi-Lagrangian diagnostics 3. *Mon. Wea. Rev.*, **104**, 3–14.

Kung, E. C., 1966a: Kinetic energy generation and dissipation in the large-scale atmospheric circulation. *Mon. Wea. Rev.*, **94**, 67–82.

——, 1966b: Large-scale balance of kinetic energy in the atmosphere. *Mon. Wea. Rev.*, **94**, 627–640.

——, 1967: Diurnal and long-term variations of the kinetic energy generation and dissipation for a five-year period. *Mon. Wea. Rev.*, **95**, 593–606.

——, 1969: Further study on the kinetic energy budget. *Mon. Wea. Rev.*, **97**, 573–581.

——, 1970: On the meridional distribution of source and sink terms of the kinetic energy balance. *Mon. Wea. Rev.*, **98**, 911–916.

——, and W. E. Baker, 1975: Energy transformations in middle-latitude disturbances. *Quart. J. Roy. Meteor. Soc.*, **101**, 793–815.

——, and J. B. Behrens, 1974: An analysis of subsynoptic scale turbulent energy with upper-air wind profiles. *J. Meteor. Soc. Japan*, **52**, 218–229.

——, and T. L. Tsui, 1975: Subsynoptic-scale kinetic energy balance in the storm area. *J. Atmos. Sci.*, **32**, 729–740.

Kurihara, Y., 1961: Accuracy of winds-aloft data and estimation of error in numerical analysis of atmospheric motions. *J. Meteor. Soc. Japan*, **39**, 331–345.

Lettau, H. H., 1959: Wind profile, surface stress and geostrophic drag coefficient in the atmospheric surface layer. *Advances in Geophysics*, Vol. 6, Academic Press, 241–255.

Lorenz, E. N., 1967: The nature and theory of the general circulation of the atmosphere. WMO 218, Tech. Publ. 115, World Meteorological Organization, 161 pp.

Margules, M., 1910: On the energy of storms. *Smithson. Misc. Collect.*, **51**, No. 4, 533–595.

McInnis, D. H., and E. C. Kung, 1972: A study of subsynoptic scale energy transformations. *Mon. Wea. Rev.*, **100**, 126–132.

Newton, C. W., and E. Palmen, 1963: Kinematic and thermal properties of a large amplitude wave in the westerlies. *Tellus*, **15**, 99–119.

O'Brien, J. J., 1970: Alternative solutions to the classical vertical velocity problem. *J. Appl. Meteor.*, **9**, 197–203.

Oort, A. H., 1964: On estimates of the atmospheric energy cycle. *Mon. Wea. Rev.*, **92**, 483–493.

Pearce, R. P., 1974: The design and interpretation of diagnostic studies of synoptic-scale atmospheric systems. *Quart. J. Roy. Meteor. Soc.*, **100**, 265–285.

Shuman, F. G., and J. B. Hovermale, 1968: An operational six-layer primitive equation model. *J. Appl. Meteor.*, **7**, 525–547.

Smith, P. J., 1969: On the contribution of a limited region to the global energy budget. *Tellus*, **21**, 202–207.

——, 1973a: The net generation of large-scale available potential energy by subgrid-scale processes. *J. Atmos. Sci.*, **30**, 1714–1717.

——, 1973b: The kinetic energy budget over North America during a period of major cyclone development. *Tellus*, **25**, 411–423.

——, 1973c: Mid-latitude synoptic-scale systems: Their kinetic energy budgets and role in the general circulation. *Mon. Wea. Rev.*, **101**, 757–762.

Vincent, D. G., and L. N. Chang, 1973: Some further considerations concerning energy budgets of moving systems. *Tellus*, **25**, 224–232.

——, W. R. Gommel and L. N. Chang, 1974: Kinetic energy study of Hurricane Celia, 1970. *Mon. Wea. Rev.*, **102**, 35–47.

Wooldridge, G. L., 1972: Effects of internal gravity waves on energy budgets and the vertical transport of angular momentum over mountainous terrain. *Mon. Wea. Rev.*, **100**, 177–188.